European Journal of Applied Sciences – Vol. 13, No. 05
Publication Date: September 14, 2025
DOI:10.14738/aivp.1305.19348.
Samosir, J. T. & Cui, W. (2025). On-chip Optofluidic Sensors for Marine Environmental Monitoring: Fundamentals, Current Progress, and Future Directions. *European Journal of Applied Sciences, Vol - 13(05).* 96-116.

SERVICES FOR SCIENCE AND EDUCATION

On-chip Optofluidic Sensors for Marine Environmental Monitoring: Fundamentals, Current Progress, and Future Directions

Justin Todo Samosir
Zhejiang Engineering Research Centre of Micro/Nano-Photonic/Electronic System Integration, Hangzhou, Zhejiang 310030, China, Department of Electronic and Information Engineering, School of Engineering, Westlake University, Hangzhou, Zhejiang 310030, China, and Department of Mechanical Engineering, Faculty of Electrical and Electronic Engineering, Northwestern Polytechnical University, Xi'An 710072, China

Weicheng Cui
Zhejiang Engineering Research Centre of Micro/Nano-Photonic/Electronic System Integration, Hangzhou, Zhejiang 310030, China and Department of Electronic and Information Engineering, School of Engineering, Westlake University, Hangzhou, Zhejiang 310030, China

ABSTRACT

Marine observing increasingly demands sensors that are compact, low-power, and reliable under salinity, temperature, pressure, and biofouling. Conventional instruments meet many performance targets but remain bulky, energy-intensive for dense, long-duration deployment. On-chip optofluidic, which integrates microfluidic with optical transduction, offers a path to miniaturize ocean sensing. This review explains the sensing principles relevant to seawater such as refractive index, absorbance/colorimetry, fluorescence, surface plasmon resonance (SPR/LSPR), with brief notes on elastic scattering and fluidic manipulation. It highlights the key seawater parameters (salinity, temperature, pH/alkalinity, nutrients, dissolved metals, and selected contaminants) along with types of architectures by integration levels, focusing on on-chip optical transducers and clearly separating them from microfluidics coupled to external optical cells. In addition, this paper also summarizes representative progress from 2015-2025 across key seawater physicochemical and contaminants targets). Finally, it outlines a conceptual on-chip design that integrates three measurands (urea, salinity, and microplastics) on a single chip, illustrating further capability of optofluidic technology. Overall, the article provides a concise path from principles to field readiness for optofluidic sensors in marine environmental monitoring.

Keywords: On-chip optofluidic, marine environmental monitoring, microfluidics, optical transduction, seawater parameter.

INTRODUCTION

Monitoring seawater quality is critical for ensuring sustainable fisheries and mitigating the impacts of environmental change [1]. The ocean acts as a vital buffer for the planet, absorbing nearly 25% of anthropogenic CO_2 emissions and regulating global temperatures, while

supporting millions of marine species [2-4]. However, human activities have increasingly stressed marine environments through chemical pollution, industrial waste, and the influx of microplastics. Each year, an estimated 8 million tons of plastic enter the ocean, while nutrient runoff has contributed to more than 400 hypoxic "dead zones" worldwide, severely threatening biodiversity and long-term ecosystem stability [5,6]. As these threats escalate, the need for accurate, real-time monitoring of seawater parameters has become increasingly urgent to inform timely interventions and safeguard marine health [7].

Conventional seawater monitoring relies on large, bulky instruments that, while precise, often require significant power, frequent maintenance, and skilled operation. Such systems can be cost-prohibitive and logistically challenging to deploy in remote or long-term field settings [8-10]. For example, the SAMI-pH sensor (Sunburst Instruments) is an autonomous spectrophotometric pH analyzer (55 ×15 cm) used on mooring platforms, offering high precision in carbonate system monitoring but limited to shallow depths (< 60 bar) due to its size and pressure tolerance [11]. Similarly, the SUNA V2 nitrate sensor (Sea-Bird Scientific) uses UV absorbance (10 mm pathlength) to measure nitrate in situ at 0.5-2.0 μM precision, but remains relatively power-intensive (7.5 W) and bulky (2.5-5.1 kg and ~1.7 L displacement) for widespread deployment [12]. These limitations have driven the development of miniaturized, portable, and energy-efficient alternatives capable of delivering comparable performance[9].

In recent years, optofluidic microsensors have emerged as a compelling solution, combining high sensitivity in a compact design and leveraging extremely small sample volumes, leading to wellbalanced performance [13]. Optofluidic microsensors leverage the interaction of light and microscale fluid handling to measure key marine parameters such as pH, salinity, nutrients, dissolved metals, dissolved gases and other micro-contaminants, [11, 14-18]. By combining photonic structures (waveguides, interferometers, and resonators) with microfluidic channels, these devices can achieve high sensitivity while requiring only microliters of sample. Their small size, low power demand, and compatibility with chip-level integration make them highly attractive for autonomous and distributed marine monitoring networks [19,20]. Recent prototypes have already demonstrated applications ranging from nutrient detection and chlorophyll fluorescence monitoring to pH and dissolved CO_2 analysis, moreover capable of monitoring 2 different measurands at the same time, such as Beaton et al., (2022) which measures phosphate and nitrate [21].

In this review, 'optofluidic' refers to on-chip optical transducers that interrogate the analyte within micro-engineered channels or cavities. Microfluidic systems that route seawater to external optical cells (e.g., liquid-waveguide capillaries or bench spectrometers) are discussed for context but, due to incomparable performance indicators, are excluded from the representative progress table (**Table 2**). Moreover, the focus analytes in the benchmarking section are limited to physicochemical components of seawater (e.g., pH, salinity, dissolved metals) as well as contaminants including microplastics and related pollutants.

This review first introduces the fundamentals of optofluidic technology, outlining how optics and fluids interact and the core sensing mechanisms of refractive index, absorbance, fluorescence, SPR/LSPR, and scattering, together with fluidic manipulation strategies. It then situates these mechanisms in the marine environment, emphasizing physicochemical and

contaminant parameters while briefly noting biological factors. The discussion proceeds to sensor architectures, distinguishing on-chip, off-chip, and hybrid approaches and comparing their performance. Representative sensing mechanisms reported in the literature are subsequently examined, followed by a synthesis of progress from 2015–2025 across different analytes and deployment modes. Finally, the review concludes with future capabilities through a conceptual multi-measurand on-chip design, illustrated in the context of monitoring the Citarum River.

FUNDAMENTALS OF OPTOFLUIDIC TECHNOLOGY

Optofluidic integrates optics and fluidics into a versatile platform. In this approach, fluids can shape, guide, or tune light, while light can also manipulate fluids or their contents [22]. In the opticsmanipulating-fluid regime, light can manipulate, position, and transport fluid-borne particles without physical contact. The most iconic example is the optical tweezer, where a tightly focused laser beam traps microscopic objects through two competing photon-derived forces. The gradient force pulls particles toward the region of highest intensity at the beam focus, while the scattering force pushes them downstream in the beam-propagation direction. Whether a particle is trapped or pushed away depends on user-controlled parameters such as laser power and the numerical aperture of the focusing lens. By adjusting these parameters, an operator can switch between stable trapping and pure radiation pressure (see **Figure 1**)[23,24].

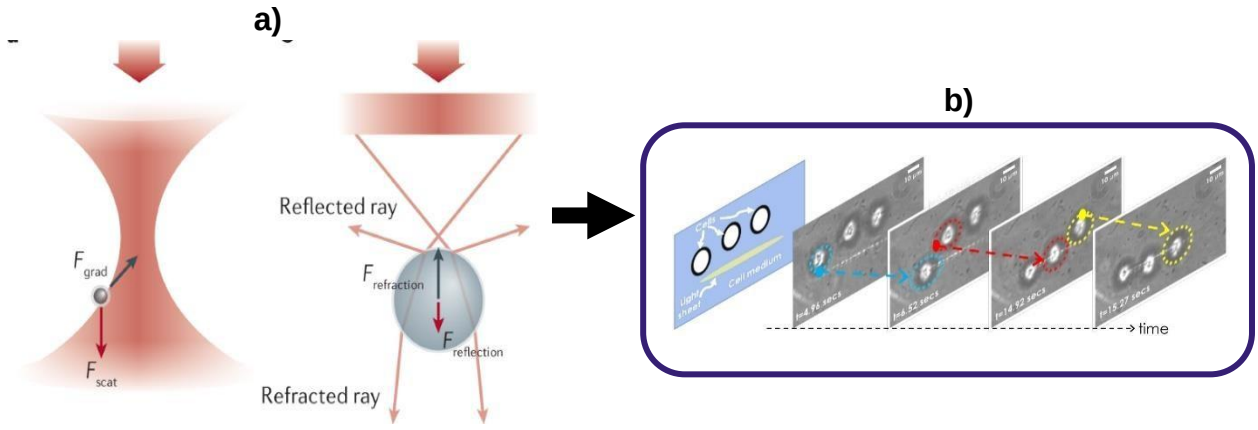

Figure 1: Schematic illustration of optical tweezer mechanism. (a) Optical tweezers trap particles by balancing two light-derived forces: scattering pushes along the beam, while the gradient pulls toward the focus. For larger particles, reflection and refraction also generate restoring forces that stabilize the trap [25](b) Lightsheet Optical Tweezers (LOT) for trapping freely moving HeLa cells suspended in cell medium (DMEM). The randomly moving cells were trapped one-by-one and aligned in a line[26].

In the fluids-manipulating-optics regime, the liquid itself modifies light behaviour by altering its refractive index, absorbing specific wavelengths, or scattering the beam inside an optofluidic channel [27]. Because the sensing regions are micro-engineered, flow is almost always laminar. This is due to the Reynolds number that shrinks with channel size, suppressing turbulence and stabilizing optical paths. The microscale geometry further confers advantages such as rapid thermal equilibration (high surface-to-volume ratio) and faster molecular diffusion, which scales with channel width [28]. These benefits underpin the broader “lab-on-a-chip”

movement, where complete wet-chemistry workflows can be miniaturized onto palm-sized cartridges.

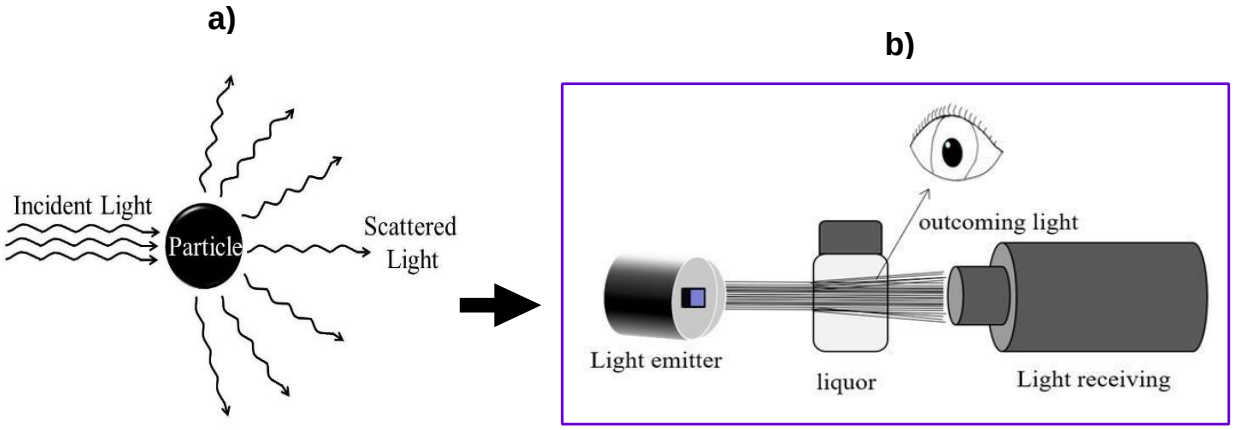

Figure 2: Illustration of Tyndall effect. (a) A particle scatters incident light, producing the characteristic sideways glow [29]. (b) Principle diagram of sauce-flavor liquor identification based on the Tyndall phenomenon [30].

The physical concepts are easily illustrated by a simple laser-pointer demonstration of the Tyndall effect (see **Figure 2**). When light passes through the liquor, colloidal particles scatter it, producing the Tyndall effect visible to the eye and measurable by the detector. Because liquor colloids contain particles of varying sizes, incident light undergoes multiple scattering events, with each particle both scattering and receiving scattered rays [30]. Optofluidic sensors exploit the same physics which is monitoring scattering, absorption, refractive index, or fluorescence changes to quantify turbidity, detect microplastics, or track nutrient chemistry in seawater [22]. Because many recent studies emphasize dissolved or suspended targets in water rather than manipulating the water itself, fluidenabled optical sensing has become the dominant theme in modern optofluidic research [31].

The six primary optofluidic mechanisms exploited in marine sensing are summarized in **Figure 3**. Each approach leverages distinct light–fluid interactions, allowing detection of solutes, particulates, or biomolecules with high sensitivity. The subsections below elaborate on these mechanisms in detail.

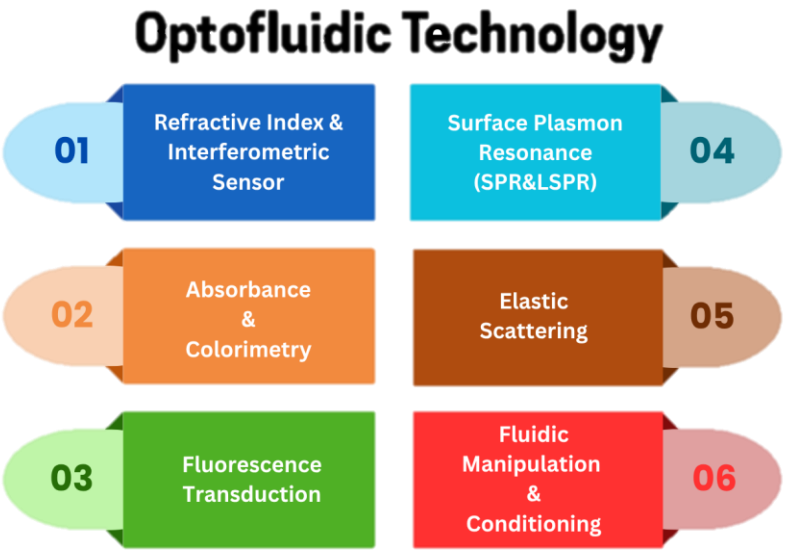

Figure 3: Schematic overview of core optofluidic sensing mechanisms for marine applications (refractive index & interferometric, absorbance & colorimetry, fluorescence, SPR&LSPR, scattering, and fluid manipulation)

Refractive Index & Interferometric Sensors

Refractive index sensing can detect analytes in their natural state without labels, making it useful for monitoring processes without disturbing them. In interferometers such as the Fabry-Perot cavity, this manifests as a measurable phase difference(Equation (1))[32].

$$\varphi = \frac{4\pi nd}{\lambda} \tag{1}$$

Where: φ – phase difference, $\boldsymbol{\lambda}$ – wavelength of the incident light wave, n – refractive index of the medium, and d – separation distance [33]

In physical terms, the sample liquid alters the optical velocity of the beam, causing a measurable delay relative to the reference arm. When the two paths recombine, any index difference produces measurable fringe shifts in wavelength or intensity. The higher the solute concentration, the larger the shift [34].

Absorbance & Colorimetry

A reagent converts the target chemical into a dye that absorbs at a known wavelength. The microchannel thus acts as a miniature cuvette, and the transmitted intensity follows the Beer–Lambert law (Equation (2)):

$$A = \varepsilon lc \tag{2}$$

where: A – absorbance, ε – molar absorption coefficient, l – optical path length, c – analyte concentration [35]. Absorbance is also expressed in terms of light intensities (Equation (3)):

$$A = -log_{10}\left(\frac{I}{I_0}\right) \tag{3}$$

where*:* I_0 – incident intensity, I – the transmitted intensity [35].

In practice, a micro-channel serves as a miniaturized cuvette for absorbance detection. Longer optical paths amplify sensitivity, so designs often serpentine geometries that not only extend the beam path but also enhance fluid mixing efficiency [36,37]. This miniaturized strategy enables tracelevel nutrient detection in seawater, where optofluidic chips can effectively replace bulky spectrophotometers [38].

Fluorescence Transduction

Fluorescence occurs when molecules absorb excitation light and re-emit at a longer wavelength. Fluorogenic chemistries enhance sensitivity because fluorescence appears only after reaction with the target [39,40]. According to prior literature review, 33% of the publications used fluorescencebased biosensors [41]. For example, in marine sensing, Rhodamine-based fluorescence has been applied for mercury detection under high-salinity conditions, demonstrating suitability for integration into a digital microfluidic platform [42].

Surface Plasmon Resonance (SPR&LSPR)

Surface plasmon resonance (SPR) arises from charge-density oscillations at the interface between a metal and a dielectric with opposite permittivity signs, most commonly gold or silver in contact with water. These oscillations are coupled to a transverse-magnetic (TM) electromagnetic wave that is bound to the interface and decays evanescently into both media. The propagation constant of the surface plasmon wave depends on the dielectric constant of the metal and the refractive index of the adjacent medium, with resonance supported when the metal permittivity is sufficiently negative [43]. This mechanism has been widely developed in oceanography, for example, an in situ SPR system using special optical fibres for measuring salinity based on refractive index determination [44] or SPR biosensor system to measure dissolved domoic acid (DA) [45].

Elastic (Mie) Scattering & Fluidic Manipulation

Elastic light scattering and fluidic conditioning are complementary strategies in marine optofluidic sensing. Elastic light scattering underpins optical particle sizing by relating optical measurements to particle properties such as size, shape, and refractive index. Classical analysis has been dominated by Mie theory, which applies to spherical, homogeneous, and isotropic particles in non-absorbing media. Because real particles are often non-spherical or inhomogeneous, more advanced scattering theories and computational methods have been developed, including surface-based, volume-based, and multiple scattering approaches [46]. For example, a study showed that combining scattering with Raman spectroscopy in a microfluidic cuvette enables simultaneous identification of microplastic type and particle size [47].

Fluidic conditioning and manipulation refer to the set of techniques used to prepare, stabilize, and precisely control fluid samples inside microchannels so that optical sensing remains accurate and reproducible. At the microscale, flows are typically laminar (low Reynolds number), which allows predictable transport but requires careful handling of mixing [48]. Manipulation tools such as microvalves and micromixers regulate sample volumes, fold and swirl reagents for rapid mixing [49].

MARINE ENVIRONMENT CONTEXT

The ocean supports an extraordinary breadth of biodiversity and serves as a vast, natural testing ground for optofluidic sensors, especially in monitoring and pollutant prevention [50]. Ocean sensing spans in biological (e.g. phytoplankton, algae, etc), but this review focuses further on physicochemical parameters such as salinity, pH, dissolved gases, and nutrients, and contaminants, as the baselines of marine systems [51].

Physicochemical and Contaminants Parameters

The ocean acts as an immense reservoir of chemical and physical signals, and miniaturized optofluidic sensors now enable their detection in situ. Continuous monitoring of fundamental parameters is essential, since these baselines the ocean biogeochemical cycle, pollution, and forecasting marine disaster [50] (see **Figure 4**)

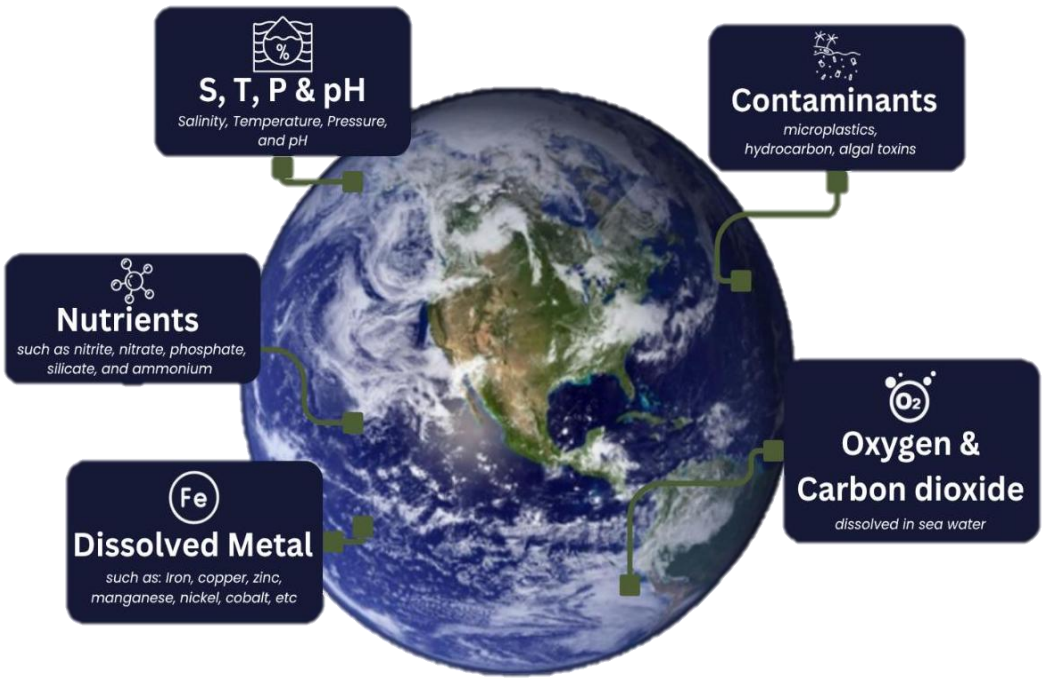

Figure 4: Key physicochemical and contaminants parameters of the marine environment addressed by optofluidic sensors.

The following subsections summarize how optofluidic devices have been tailored for key ocean variables.

Core Physical Variables (Salinity, Temperature, Pressure, pH)

Accurate measurement of temperature, salinity, and pressure (TSP) underpins the interpretation of marine biogeochemistry, circulation, and acoustic transmission [52]. As core density-driving variables, TSP also regulate regional sea-level change, vary systematically with depth, and are widely used in climate change research [53,54]. Optical fibre sensors (OFSs) exploit the dependence of seawater refractive index on TSP, as described by empirical formulations [55]. By transducing TSP-induced RI changes into optical signals— through resonance, phase, or absorption shifts—OFSs enable in situ sensing. Multiparameter designs

such as fibre Bragg gratings, interferometers, SPR, and microfiber sensors are increasingly applied to decouple cross-sensitivity among T, S, and P [52]. In addition, pH is a critical baseline parameter, with ocean acidification lowering surface pH by ~0.1 units, threatening carbonate chemistry. An autonomous spectrophotometric pH sensor now enables high-precision measurements from the surface to 6000 m [11].

Nutrients

Nutrients such as nitrate, phosphate, silicate, and ammonium fuel ocean productivity and help define ecosystem structure. Optofluidic platforms adapt classical wet-chemistry assays—whether absorbance-based colorimetry or fluorescence—into microfluidic chips, where reagents mix with the sample to generate optically detectable products. These approaches drastically reduce reagent volumes while allowing in situ deployment. Nutrient monitoring matters for fisheries management and predicting harmful algal blooms. As an example, microfluidic Griess-based nitrate sensors have been successfully deployed on moored platforms, tracking seasonal nutrient fluctuations with micromolar sensitivity [56-59].

Dissolved Metals

Trace metals are essential micronutrients in marine systems but can become toxic when present at elevated concentrations. Elements such as Cu, Co, Ni, and Cd are required for phytoplankton growth, and as nutrient-type metals their concentrations are typically lowest in surface waters—where they are assimilated by primary producers or adsorbed onto particles—and increase with depth through particle decomposition and dissolution [60,61]. Other dissolved metals, such as manganese (Mn) and iron (Fe), are also critical to monitor given their roles in ocean biogeochemistry. Despite their key role in biogeochemical cycling, dissolved trace metals occur at extremely low concentrations, making seawater samples highly susceptible to contamination if not handled carefully during sampling and analysis [62]. Optofluidic technologies support this effort by enabling spectrophotometric absorbance or colorimetric detection, miniaturizing classical assays into compact platforms. Recent in situ studies have demonstrated high sensitivity for dissolved metal detection while significantly reducing reagent consumption, highlighting the promise of optofluidic for long-term ocean monitoring [15].

Dissolved Gases (O_2, CO_2)

Investigating the links between climate change—particularly ocean deoxygenation—and the socio-economic impacts on fisheries is essential for determining sustainable levels of fish stock exploitation that balance human needs with marine ecosystem health. At the same time, rising atmospheric CO_2 from fossil fuel combustion, deforestation, and land-use practices is driving wholesale increases in seawater CO_2 and dissolved inorganic carbon, reducing pH, and altering the acid–base chemistry of estuarine, coastal, and open-ocean waters [63,64]. One in situ example is the SAMI-CO_2 sensor, known for its long-term stability, low reagent use, and precise, real-time measurements due to its robust design and optical efficiency [65].

Contaminants

Plastic pollution has emerged as one of the most urgent global environmental issues, severely impacting marine ecosystems and human health. Microplastics enter the marine food chain primarily through ingestion by marine organisms, which mistake them for food, and through

trophic transfer across species [66,67]. One study concludes that integrating microfluidics, Raman spectroscopy, and machine learning can streamline microplastic sampling and identification, improving both the efficiency and accuracy of marine microplastic analysis [18].

ARCHITECTURE OF OPTOFLUIDIC SENSOR

Throughout the literature, notable inconsistencies appear in how the term "optofluidic microsensor" is defined. Broadly, three distinct interpretations emerged. The first describes off-chip optofluidic microsensors, where microfluidic manipulation is performed on a chip but optical detection takes place entirely outside the chip architecture. The second refers to hybrid optofluidic microsensors, which combine microfluidics and certain optical components on the chip but still depend on external optical modules (such as a liquid waveguide capillary cell /LWCC) for part of the sensing process, as exemplified by Yang et al. (2024). The third and most integrated approach defines on-chip optofluidic microsensors as platforms in which both optical manipulation and microfluidic sample handling occur entirely within a single chip. Understanding and clearly distinguishing these categories is essential to avoid bias when comparing device performance and to build a consistent definition that can guide future research and innovation in field.

"On-chip" Optofluidic

On-chip optofluidic sensors integrate both the optical detection components and the components and the microfluidic sample-handling channels onto a single microfabricated substrate, often using silicon, glass, or polymer platforms. Light sources, waveguides, resonators, or interferometers are patterned directly alongside the fluidic network as one compact architecture. The main trade-off is that on-chip optical path lengths are inherently short (typically in milli meter to centimeter range) limiting absorbance sensitivity compared to long-path systems. Nevertheless, on-chip designs excel in field-deployment, autonomous monitoring where size, power, and mechanical stability are critical [68].

"Off-chip" Optofluidic

Off-chip optofluidic architectures separate the optical detection path from the microfluidic reaction or sample preparation unit. The microfluidic platform may prepare or condition the sample, which is then routed to an external optical cell for measurement (such as cuvette, flow-through chamber, or liquid waveguide capillary cell/LWCC). This arrangement allows the use of extended optical path lengths (tens of centimeters) and specialized detection optics that cannot be easily miniaturized onto a chip. For instance, LWCCs use total internal reflection inside a Teflon AF capillary to guide light through the sample with minimal loss, enabling detection limits in the nanomolar range for colorimetric assays. However, off-chip systems are bulkier, require more precise alignment, consume larger sample volumes, and are less rugged for deployment in mobile or harsh marine environment [69].

Hybrid

Hybrid designs combine on-chip and off-chip optical modules to leverage the strengths of both approaches. In these systems, part of the optical measurement occurs within an integrated on-chip cell (e.g., a short-path microfabricated waveguide or absorption chamber) for rapid, low-volume detection, while a secondary off-chip optical unit (often an LWCC) provides a longer path for enhanced sensitivity when needed. A notable example is the nitrite/nitrate analyzer

by Yang et al. (2024), which integrates a 5 cm internal absorption cell on the microfluidic chip and a 20 cm external LWCC, achieving an order-of-magnitude improvement in limit of detection compared to on-chip only. While hybrids can significantly expand dynamic range and sensitivity, they also introduce complexity in fluid routing, optical coupling, and calibration. As a result, their footprint, power requirements, and deployment ruggedness may more closely resemble off-chip systems than fully integrated designs, making direct performance benchmarking across architectures inherently challenging [70]. To ensure consistency across the literature, it is logical to establish a uniform baseline when defining sensor architectures. The field of optofluidic microsensors has often blurred the boundary between on-chip and off-chip approaches, making a clear framework essential for accurate benchmarking. By distinguishing these categories, readers can better understand the degree of integration achieved in different platforms and how this impacts performance and deployment readiness
To illustrate these contrasts in a concretely, two representative examples are highlighted from prior studies, which respectively showcase on-chip, off-chip, and hybrid implementations. These cases serve as reference points for clarifying the terminology and guiding further discussion on what constitutes a fully integrated optofluidic microsensor (see **Table 1**).

Table 1: Performance comparison between on chip, off chip and hybrid optofluidic

Feature	**Zhang et al., 2016 (On-Chip) [68]**	**Yang et al., 2020 (Off-Chip) [69]**	**Yang et al., 2024 (Hybrid) [70]**
Architecture Type	Fully on-chip; MZI structure is integrated into an optical waveguide	SIA (Sequential Injection Analysis) microfluidic chip with external LWCC and spectrophotometric detection	Hybrid: on-chip absorption cell + off-chip LWCC
Marine Sample Used	Yes (seawater salinity and temperature)	Yes (seawater analyzed for in situ and online at Pearl River estuary and northern South China Sea)	Yes (laboratory analysis from South China Sea and then InSitu)
Optical Path Length	Channel dimension 16 × 1 × 0.075 mm; sensing arm 24.29 mm	External LWCC 10 cm path length (external to chip)	Internal 5 cm (absorption cell); LWCC external 20 cm
Sensitivity / LoD	Salinity sensitivity 215.7 nm/RIU; temperature 0.519 nm/°C	1.4 μg L^{-1} (≈ 14.7 nM) phosphate with 23 μL max reagent per assay	Internal 5 cm = 0.0150 μM LWCC 20 cm = 0.0936 μM
Footprint & Portability	Millimeter-scale footprint, making it highly portable compared to external-cell systems	Larger footprint (53 cm height and 17.5 cm in diameter), 8 kg (less portable)	Portable, connection parts of the analyzer are 3D-printed.
Sample Volume	Not explicitly specified, however the channel dimension indicates 1.2 μL (channel restricted only)	Tube looper volume options: 1 mL (0.8 mm ID × 1989 mm length) or 0.3 mL (1 mm ID × 382 mm length	Not explicitly specified; the system employs two 1 mL syringe pumps, which define the upper bound of sample handling per cycle
Alignment / Deployment	On-chip alignment; not fieldpackaged	Delicate optical alignment, extern LWCC, bulky, but proven in real deployments	External LWCC (20 cm) coupled by screw joint; easy assembly/replacement

SENSING MECHANISM OF OPTOFLUIDIC SENSOR

To provide a clear reference frame, this section adopts the compact ridge-waveguide layout of Barshilia et al. (2020) as an illustrative exemplar as provided in **Figure 5**. Barshilia et al. present

a simple, low-cost, and scalable optofluidic refractive-index (RI) sensor based on a planar optical waveguide (WG) integrated with a microfluidic channel [71].

The device is assembled without lithography or vacuum processing, which enhances manufacturability and throughput. Illumination is provided by a stable light-emitting diode (LED) and detection by a photodiode, enabling straightforward, real-time intensity readout. The authors report an RI resolution on the order of 5.65 x 10^{-4} RIU, indicating competitive performance for routine measurements with inexpensive hardware. Structurally, the sensor employs a suspended planar WG formed by bonding a borosilicate cover glass (serving as the guiding layer) to a glass substrate while leaving an air gap underneath. This trapped-air layer produces a strong index contrast that confines light within the guide and minimizes leakage into the substrate (see **Figure 5a,5c**).

A cyclic olefin copolymer (COC) microfluidic module is mounted above the WG to create the sensing region. In the longitudinal direction of light propagation, the platform is partitioned into three serial zones: regions 1 and 3 are clad by COC (with n ≈ 1.56), whereas the central region 2 is a liquid microchannel whose refractive index reflects the analyte solution (typically n ≈ 1.333-1.373). The sensing principle is intensity-based and relies on interfacial mode mismatch. When light of input intensity I_{in} is coupled into the WG and traverses regions 1, 2, and 3, the guided mode adapts to the local cladding index (see **Figure 5b**). Because the modal profile supported by the COC-clad sections differs from that in the liquid-clad section, transitions at the 1|2 and 2|3 interfaces induce coupling losses whose magnitude depends on the solution RI in region 2. Variations in analyte concentration therefore modulate the effective index and field overlap, altering the transmitted intensity measured as I_{out}. Notably, because the transduction arises from discrete interfacial coupling rather than cumulative propagation effects, the sensitivity is effectively independent of total waveguide length [71]. (see **Figure 5d**)

In other words, as light crosses from the COC-clad sections into the liquid-clad window and back, the guided mode reshapes because the cladding index changes; this mismatch at the two boundaries sheds some power into radiation, so the transmitted intensity drops by an amount that tracks the liquid's refractive index sampled by the evanescent field. The evanescent field is the exponentially decaying portion of the guided mode that penetrates a short distance (tens to hundreds of nanometers) into the liquid, providing the interaction volume that makes the sensing possible [72]. Beyond RI via interfacial mismatch, the same waveguide–microchannel platform also supports evanescent-field readouts—absorbance, fluorescence, scattering, etc—standard methods that vary in transduction (amplitude, phase, resonance) but share the same guided-field/liquid interaction [7375].

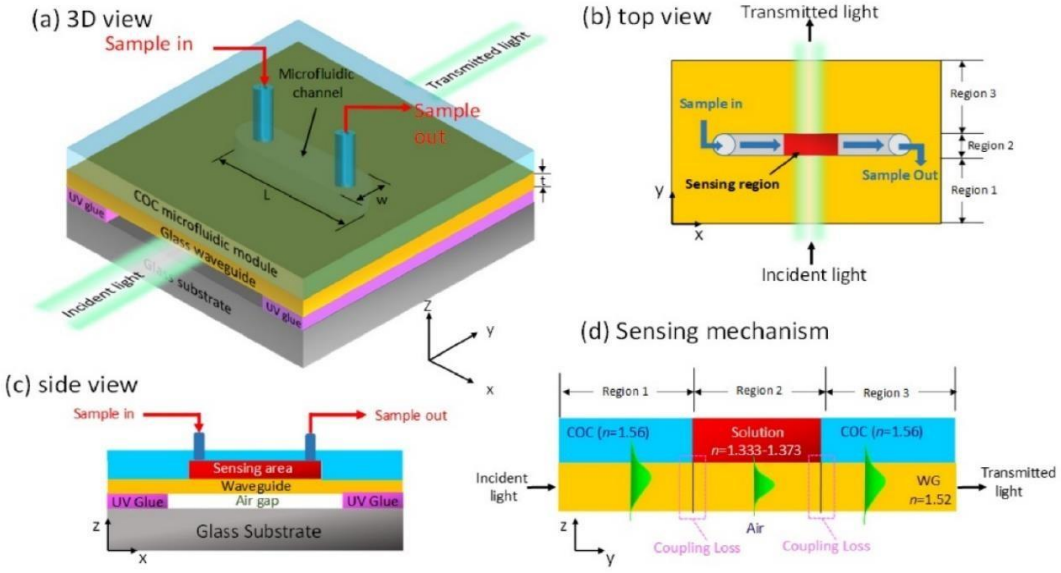

Figure 5: Diagrammatic representation of the proposed optofluidic waveguide refractive index (WG RI) sensor, including a glass substrate, a glass WG and a microfluidic channel. (a) 3D view. (b) Top view. (c) Side view. (d) Sensing mechanism of the WG RI sensor. COC: cyclic olefin copolymer.

REPRESENTATIVE PROGRESS (2015-2025)

Representative progress in on-chip optofluidic marine sensing (2015–2025). Entries are grouped by analyte class (core physical variables, nutrients, dissolved metals, dissolved gases, pollutants). Inclusion criteria: (i) peer-reviewed, English-language article; (ii) on-chip optofluidic sensor (optical transduction integrated with microfluidics; hybrid/off-chip excluded); (iii) evaluation of seawater (in situ, experimental sampling, or properties conditioning); (iv) published 2015–2025 (see **Table 2**).

Table 2: Representative On-chip Optofluidic Sensor Studies for Seawater Physicochemical and Contaminants Parameters (2015–2025)

Author	Year	Analytes	Optical transduction	Deployment Mode & Depth tested	Endurance	Sample consumption
Yin et al [11]	2021	pH	Absorbance/Colorimetric/ Spectrophotometry	6000 m using Kongsberg	1-2 months	~700 µL seawater + 3
				Seaglider, Autosub Long range, and the Liquid Robotics Waveglider		µL dye per measurement
Zhang et al [68]	2016	Salinity and Temperature	Refractive Index (Mach–Zehnder interferometer /MZI)	Laboratory demonstration only	Short-term experimental runs	Very low, indicated by 1.2 µL volume (channel restricted only)
Grand et al [57]	2017	Phosphate	Absorbance/Colorimetric/ Spectrophotometry	0.5 m – 1 m using floating docks	1 – 2 months	Not specified, however 210 µL blank/standa rd flush + 350 µL sample flush per cycle (Low)

Beaton et al [21]	2022	Nitrate and Phosphate	Absorbance/Colorimetric/ Spectrophotometry	2100 - 4800 m using CTD rosette and PROVOR profiling float	Several thousand measurements before filter replacement	< 1 mL
Geißler et al [15]	2021	Dissolved Mn (II) (DMn)	Absorbance/Colorimetric/ Spectrophotometry	2 m using fixedframe deployment which was lowered	~ 1 month	Not specified, however reagent consumption of 63 µL per sample
Geißler et al. [76]	2017	Dissolved metal iron Fe (II) (DFe)	Absorbance/Colorimetric/ Spectrophotometry	2 m using fixedframe deployment which was lowered	9 days Insitu testing	1.26 mL of each blank, standard, and sample + 168 µL per cycle
Lai et al [65]	2018	Dissolved pCO_2	Absorbance/Colorimetric/ Spectrophotometry	35 m on a subsurface mooring. 600 – 5000 m (Delrin/Titanium Housing)	1 year	2.6 mL (water sample + reagent flush) per cycle.
Vincent et al [77]	2018	ΣNOx (nitrate + nitrite)	Absorbance/Colorimetric/ Spectrophotometry	145 m using AUV, Kongsberg Seaglider.	21 days	Not specified, however reagent use per dive reported (2.5 mL Griess + 2.5 mL buffer + 0.21 mL standard/bla nk for ~10 samples)
Gong et al [18]	2023	Small microplastics (<50 µm)	Scattering (Raman spectroscopy)	Laboratory demonstration only	Short-term experimental runs	PE (20– 27 µm and 10–45 µm) and PS (9.5–11.5 µm)
Schaap et al [78]	2021	pH & Total Alkalinity (TA)	Absorbance/ Spectrophotometry and alkalinity determination	120 m using custom-built landers	11 days	Not specified

Note: The deployed devices reported here most likely underwent extensive laboratory or experimental validation before field deployment. Some analytes are not quantitatively equally represented due to the inclusivity criteria applied in this review. In particular, studies were excluded if the sensor was not strictly on-chip optofluidic or if testing was performed exclusively in freshwater environments rather than seawater.

FUTURE CAPABILITIES

The Citarum River carries large loads of urea-derived nitrogen and fragmented plastics from the Bandung highlands to Jakarta Bay (see **Figure 6a**), creating strong chemical and particulate gradients across the river–ocean interface. A compact, fieldable node that co-measures urea, salinity, temperature, and microplastics along this plume would turn a diffuse pollution story into actionable maps. The concept targets three fixed stations at approximately 1 km, 5 km, and 15 km from the river mouth, mounted on small surface moorings or pier brackets. Each station logs locally and periodically telemeters summaries, providing spatial trend information without continuous highbandwidth links. The sensor design is inspirated by Barshilia et al. (2020) (see **Figure 6b**).

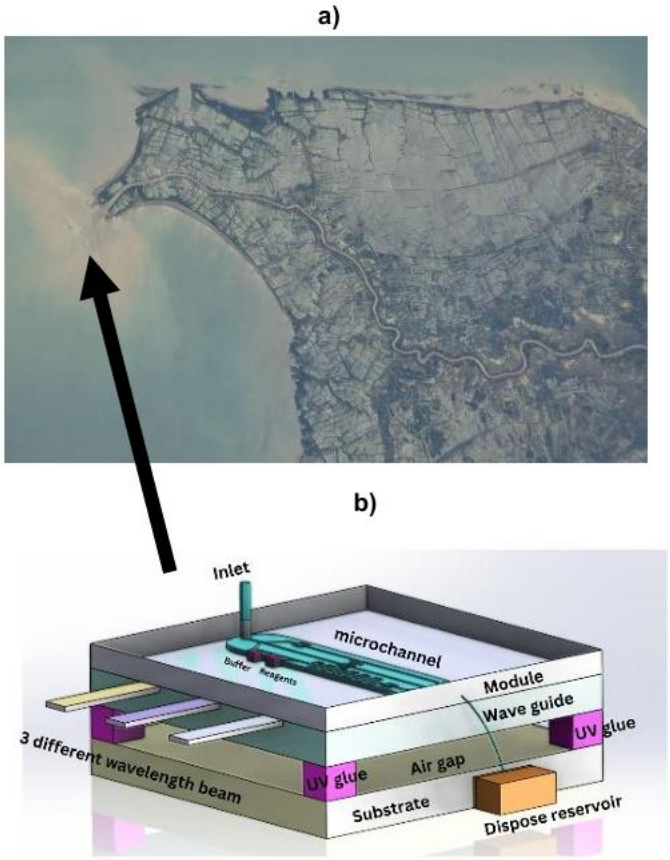

Figure 6: Proposed structural design of the optofluidic sensor chip that detects 3 parameters which are urea, salinity, and microplastics for Citarum River monitoring (a) View of Citarum River, West Java, Indonesia. (b) Structural optofluidic sensor that integrates multi-parameter sensing.

At the heart of each node is a single on-chip optofluidic sensor that splits a metered sub-microliter intake into three parallel microchannels, each crossed by a short sensing window of an integrated ridge waveguide (see **Figure 7a**). Optical isolation ribs separate the waveguides to prevent crosstalk, while a co-located thermistor provides temperature for salinity compensation. A bubble trap, rinse loop, and laminated-foil waste pouch maintain optical clarity during unattended operation.

Each branch applies a modality suited to its target. Salinity is read as a bulk refractive-index change at 1550 nm; temperature compensation yields salinity in PSU from a calibrated $n\,(T, S)$ model. Urea is converted enzymatically to ammonium and detected by indophenol (Berthelot) colorimetry with a red source near 650–700 nm; a serpentine micromixer provides residence time and homogeneous reaction. Microplastics are counted by elastic light scattering with a violet/blue source (≈405–488 nm) and a near-field photodiode positioned to collect side-scatter from particles transiting the window; optional dual-angle or polarization discrimination sharpens selectivity (see **Figure 7b**).

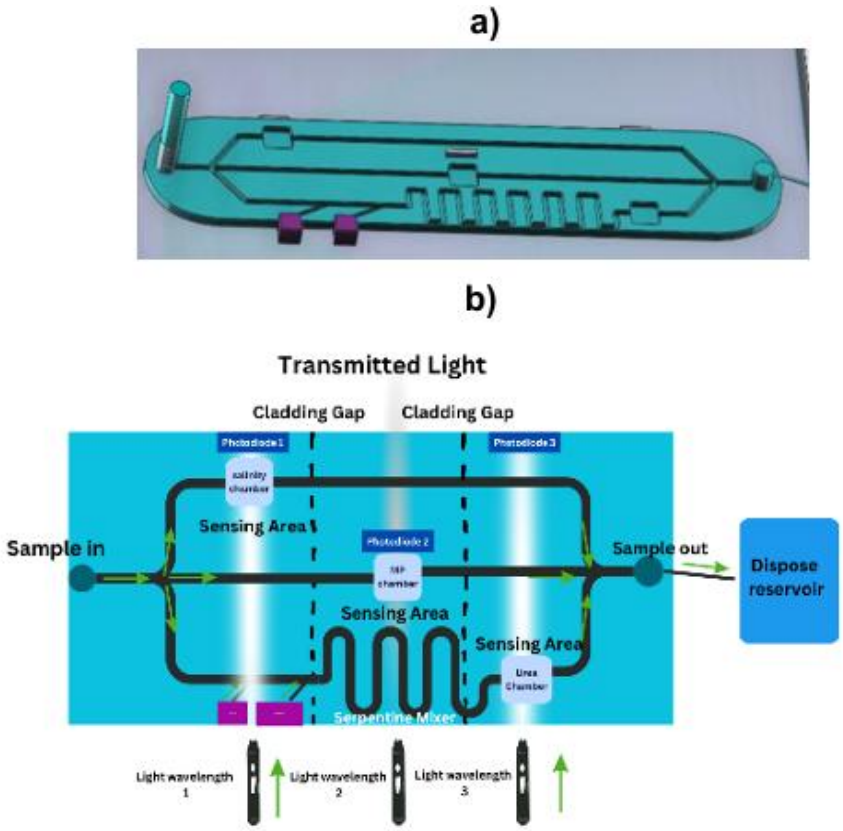

Figure 7: Proposed structural design of the optofluidic sensor chip that detects 3 parameters which are urea, salinity, and microplastics for Citarum River monitoring

Evanescent-field interrogation is central to the approach. The waveguides confine the main beam for low loss, while a nanometer-scale evanescent tail samples the flowing liquid, allowing RI, absorbance, and scattering transduction on a millimeter footprint. Avoiding free-beam propagation through turbid water reduces attenuation and bubble sensitivity and enables consistent measurements at river mouths where fouling and suspended solids are common.

Operationally, a 5–15 min cycle and modest reagent reservoirs support multi-week endurance (≥14 days at 10–30 min sampling) before servicing. Foreseeable risks (e.g., biofouling, reagent drift, bubble intrusion, and cross-sensitivity) are mitigated with antifouling coatings on exposed windows, standards/blank checks for the urea path, hydrophobic vents and pre-filters, and explicit n (T, S) compensation for the salinity path. Overall schematic operation can be found by considering **Figure 8**. Altogether, this integrated design illustrates a credible path from proof-of-concept optofluidic chips toward compact, multimodal nodes that could one day deliver robust, long-term seawater monitoring in real field environments.

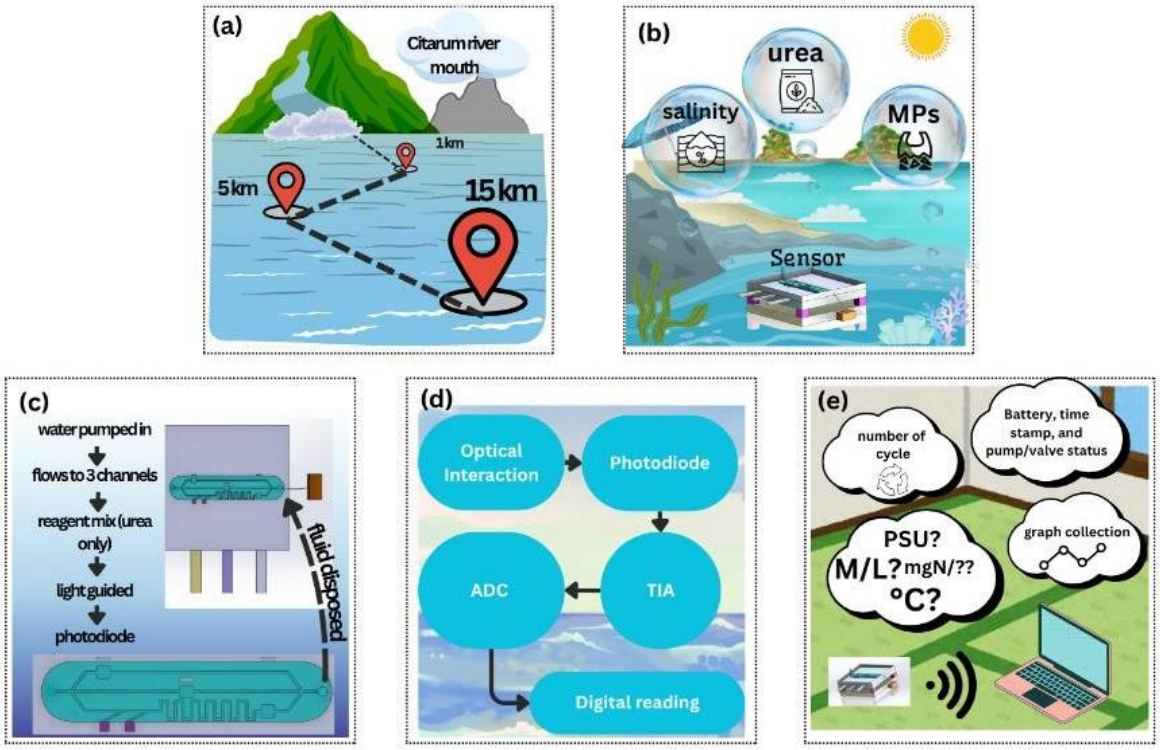

Figure 8: Operation scheme of multi-parameter sensor for Citarum River (a) Deployment range. (b) Target analysis. (c) Sample handling. (d) Signal transduction. (e) Data logging and communication

CONCLUSION

This review links the need for compact, low-power ocean instruments to the strengths of on-chip optofluidics and takes the reader from principles to practice. It explains the main optical transduction modes for seawater sensing (refractive index and interferometry, absorbance and colorimetry, fluorescence, SPR and LSPR, elastic scattering) and organizes targets into three application groups: biological, contaminants, and physicochemical parameters such as salinity, temperature, pressure, pH and alkalinity, nutrients, dissolved metals, and dissolved gases. The sensing workflow is laid out in a clear order from intake and conditioning to optical interrogation and readout, and architectures are distinguished as on-chip, off-chip, and hybrid with concrete examples. To ground the discussion, representative progress from 2015 to 2020 compares analytes, optical transduction, deployment mode and depth, endurance, and sample consumption, making recent advances and trade-offs easy to compare.

Looking forward, the multi-measurand concept that co-integrates urea, salinity, and microplastics on a single chip illustrates a practical path to compact, deployable nodes. By combining microliter-scale fluid handling with evanescent-field optical readout and simple antifouling and calibration routines, such chips could support long-duration operation on moorings, gliders, and landers. With standardized benchmarks and rugged packaging, on-chip optofluidics can move from promising prototypes to dense, distributed observatories that deliver real-time chemical intelligence across the sea.

ACKNOWLEDGEMENT

This work was completed during the first author's internship, under the guidance of the second author. This research was supported by the Scientific Research Funding Project of Westlake University (Grant No. WU2024A001), generously donated by Mr. Li Duozhu, President of Dingheng Shipping Technology Co., Ltd. The authors gratefully acknowledge this support.

References

[1] N. D. Gallo, N. M. Bowlin, A. R. Thompson, E. V. Satterthwaite, B. Brady, and B. X. Semmens, "Fisheries Surveys Are Essential Ocean Observing Programs in a Time of Global Change: A Synthesis of Oceanographic and Ecological Data From U.S. West Coast Fisheries Surveys," *Front. Mar. Sci.*, vol. 9, p. 757124, Mar. 2022, doi: 10.3389/fmars.2022.757124.

[2] N. Mayot, E. T. Buitenhuis, R. M. Wright, J. Hauck, D. C. E. Bakker, and C. Le Quéré, "Constraining the trend in the ocean CO2 sink during 2000–2022," *Nat. Commun.*, vol. 15, no. 1, p. 8429, Sept. 2024, doi: 10.1038/s41467-024-52641-7.

[3] Z. Li, M. H. England, and S. Groeskamp, "Recent acceleration in global ocean heat accumulation by mode and intermediate waters," *Nat. Commun.*, vol. 14, no. 1, p. 6888, Oct. 2023, doi: 10.1038/s41467-023-42468-z.

[4] C. Mora, D. P. Tittensor, S. Adl, A. G. B. Simpson, and B. Worm, "How Many Species Are There on Earth and in the Ocean?," *PLoS Biol.*, vol. 9, no. 8, p. e1001127, Aug. 2011, doi: 10.1371/journal.pbio.1001127.

[5] C. Thiagarajan and Y. Devarajan, "The urgent challenge of ocean pollution: Impacts on marine biodiversity and human health," *Reg. Stud. Mar. Sci.*, vol. 81, p. 103995, Jan. 2025, doi: 10.1016/j.rsma.2024.103995.

[6] P. J. Landrigan *et al.*, "Human Health and Ocean Pollution," *Ann. Glob. Health*, vol. 86, no. 1, p. 151, Dec. 2020, doi: 10.5334/aogh.2831.

[7] M. Koronides, P. Stylianidis, C. Michailides, and T. Onoufriou, "Real-Time Monitoring of Seawater Quality Parameters in Ayia Napa, Cyprus," *J. Mar. Sci. Eng.*, vol. 12, no. 10, p. 1731, Oct. 2024, doi: 10.3390/jmse12101731.

[8] Q. Yu, Y. Wang, J. Wang, and J. Dong, "Small chips, big ocean: Recent trends in microfluidic technology for marine environmental monitoring," *Trends Environ. Anal. Chem.*, vol. 46, p. e00264, June 2025, doi: 10.1016/j.teac.2025.e00264.

[9] C. Whitt *et al.*, "Future Vision for Autonomous Ocean Observations," *Front. Mar. Sci.*, vol. 7, p. 697, Sept. 2020, doi: 10.3389/fmars.2020.00697.

[10] Z. A. Wang *et al.*, "Advancing Observation of Ocean Biogeochemistry, Biology, and Ecosystems With Cost-Effective in situ Sensing Technologies," *Front. Mar. Sci.*, vol. 6, p. 519, Sept. 2019, doi: 10.3389/fmars.2019.00519.

[11] T. Yin *et al.*, "A Novel Lab-on-Chip Spectrophotometric pH Sensor for Autonomous *In Situ* Seawater Measurements to 6000 m Depth on Stationary and Moving Observing Platforms," *Environ. Sci. Technol.*, vol. 55, no. 21, pp. 14968–14978, Nov. 2021, doi: 10.1021/acs.est.1c03517.

[12] Sea-Bird Scientific, "SUNA V2 UV Nitrate Sensor — Data Sheet." Sea-Bird Scientific, Mar. 2016. [Online]. Available: https://argo.ogs.it/medargo/doc_sensori/2016_datasheet_SUNAV2-2016_0.pdf

[13] X. Fan and I. M. White, "Optofluidic microsystems for chemical and biological analysis," *Nat. Photonics*, vol. 5, no. 10, pp. 591–597, Oct. 2011, doi: 10.1038/nphoton.2011.206.

[14] G. Li, Y. Wang, A. Shi, Y. Liu, and F. Li, "Review of Seawater Fiber Optic Salinity Sensors Based on the Refractive Index Detection Principle," *Sensors*, vol. 23, no. 4, p. 2187, Feb. 2023, doi: 10.3390/s23042187.

[15] F. Geißler *et al.*, "Lab-on-chip analyser for the in situ determination of dissolved manganese in seawater," *Sci. Rep.*, vol. 11, no. 1, p. 2382, Jan. 2021, doi: 10.1038/s41598-021-81779-3.

[16] E. Luy, J. Smith, I. Grundke, C. Sonnichsen, A. Furlong, and V. Sieben, "Two chemistries on a single labon-chip: Nitrate and orthophosphate sensing underwater with inlaid microfluidics," *Front. Sens.*, vol. 3, p. 1080020, Dec. 2022, doi: 10.3389/fsens.2022.1080020.

[17] I. M. Perez De Vargas Sansalvador *et al.*, "Towards an autonomous microfluidic sensor for dissolved carbon dioxide determination," *Microchem. J.*, vol. 139, pp. 216–221, June 2018, doi: 10.1016/j.microc.2018.02.018.

[18] L. Gong, O. Martinez, P. Mesquita, K. Kurtz, Y. Xu, and Y. Lin, "A microfluidic approach for label-free identification of small-sized microplastics in seawater," *Sci. Rep.*, vol. 13, no. 1, p. 11011, July 2023, doi: 10.1038/s41598-023-37900-9.

[19] G. Testa, G. Persichetti, and R. Bernini, "Optofluidic Approaches for Enhanced Microsensor Performances," *Sensors*, vol. 15, no. 1, pp. 465–484, Dec. 2014, doi: 10.3390/s150100465.

[20] Z. Djinović, M. Tomić, and A. Kocsis, "Optofluidic Micromachined Platform for Refractive Index Measurement," *Chemosensors*, vol. 10, no. 5, p. 197, May 2022, doi: 10.3390/chemosensors10050197.

[21] A. D. Beaton *et al.*, "Lab-on-Chip for In Situ Analysis of Nutrients in the Deep Sea," *ACS Sens.*, vol. 7, no. 1, pp. 89–98, Jan. 2022, doi: 10.1021/acssensors.1c01685.

[22] C. Song and S. Tan, "A Perspective on the Rise of Optofluidics and the Future," *Micromachines*, vol. 8, no. 5, p. 152, May 2017, doi: 10.3390/mi8050152.

[23] D. G. Grier, "A revolution in optical manipulation," *Nature*, vol. 424, no. 6950, pp. 810–816, Aug. 2003, doi: 10.1038/nature01935.

[24] K. C. Neuman and S. M. Block, "Optical trapping," *Rev. Sci. Instrum.*, vol. 75, no. 9, pp. 2787–2809, Sept. 2004, doi: 10.1063/1.1785844.

[25] C. J. Bustamante, Y. R. Chemla, S. Liu, and M. D. Wang, "Optical tweezers in single-molecule biophysics," *Nat. Rev. Methods Primer*, vol. 1, no. 1, p. 25, Mar. 2021, doi: 10.1038/s43586-02100021-6.

[26] P. P. Mondal, N. Baro, A. Singh, P. Joshi, and J. Basumatary, "Lightsheet optical tweezer (LOT) for optical manipulation of microscopic particles and live cells," *Sci. Rep.*, vol. 12, no. 1, p. 10229, June 2022, doi: 10.1038/s41598-022-13095-3.

[27] G. Testa, G. Persichetti, and R. Bernini, "Optofluidic Approaches for Enhanced Microsensor Performances," *Sensors*, vol. 15, no. 1, pp. 465–484, Dec. 2014, doi: 10.3390/s150100465.

[28] C.-Y. Lee, C.-L. Chang, Y.-N. Wang, and L.-M. Fu, "Microfluidic Mixing: A Review," *Int. J. Mol. Sci.*, vol. 12, no. 5, pp. 3263–3287, May 2011, doi: 10.3390/ijms12053263.

[29] "Dispersion of light through prism -scattering | Science Class." Accessed: Aug. 21, 2025. [Online]. Available: https://scienceweem.blogspot.com/2021/06/dispersion-of-light-through-prism-and.html

[30] H. Liu *et al.*, "Quality Identification of Sauce-Flavor Liquor Based on the Tyndall Phenomenon," *Appl. Sci.*, vol. 12, no. 1, p. 53, Dec. 2021, doi: 10.3390/app12010053.

[31] D. Ozcelik, H. Cai, K. D. Leake, A. R. Hawkins, and H. Schmidt, "Optofluidic bioanalysis: fundamentals and applications," *Nanophotonics*, vol. 6, no. 4, pp. 647–661, Mar. 2017, doi: 10.1515/nanoph-20160156.

[32] A. Crespi *et al.*, "Three-dimensional Mach-Zehnder interferometer in a microfluidic chip for spatiallyresolved label-free detection," *Lab. Chip*, vol. 10, no. 9, p. 1167, 2010, doi: 10.1039/b920062b.

[33] C. Ma, D. Peng, X. Bai, S. Liu, and L. Luo, "A Review of Optical Fiber Sensing Technology Based on Thin Film and Fabry–Perot Cavity," *Coatings*, vol. 13, no. 7, p. 1277, July 2023, doi: 10.3390/coatings13071277.

[34] E. Labella and R. Gupta, "An Optofluidic Young Interferometer for Electrokinetic Transport-Coupled Biosensing," *Micromachines*, vol. 15, no. 7, p. 861, June 2024, doi: 10.3390/mi15070861.

[35] E. A. Luy, S. C. Morgan, J. J. Creelman, B. J. Murphy, and V. J. Sieben, "Inlaid microfluidic optics: absorbance cells in clear devices applied to nitrite and phosphate detection," *J. Micromechanics Microengineering*, vol. 30, no. 9, p. 095001, Sept. 2020, doi: 10.1088/1361-6439/ab9202.

[36] M. Javaid, T. Cheema, and C. Park, "Analysis of Passive Mixing in a Serpentine Microchannel with Sinusoidal Side Walls," *Micromachines*, vol. 9, no. 1, p. 8, Dec. 2017, doi: 10.3390/mi9010008.

[37] Z. Yang *et al.*, "A high-sensitivity lab-on-a-chip analyzer for online monitoring of nitrite and nitrate in seawater based on liquid waveguide capillary cells," *Lab. Chip*, vol. 24, no. 14, pp. 3528–3535, 2024, doi: 10.1039/D4LC00248B.

[38] S. Morgan, E. Luy, A. Furlong, and V. Sieben, "A submersible phosphate analyzer for marine environments based on inlaid microfluidics," *Anal. Methods*, vol. 14, no. 1, pp. 22–33, 2022, doi: 10.1039/D1AY01876K.

[39] J. R. Lakowicz, G. Freshwater, and G. Weber, "Nanosecond segmental mobilities of tryptophan residues in proteins observed by lifetime-resolved fluorescence anisotropies," *Biophys. J.*, vol. 32, no. 1, pp. 591–601, Oct. 1980, doi: 10.1016/S0006-3495(80)84992-7.

[40] J. W. Taraska and W. N. Zagotta, "Fluorescence Applications in Molecular Neurobiology," *Neuron*, vol. 66, no. 2, pp. 170–189, Apr. 2010, doi: 10.1016/j.neuron.2010.02.002.

[41] M. Herrera-Domínguez, G. Morales-Luna, J. Mahlknecht, Q. Cheng, I. Aguilar-Hernández, and N. Ornelas-Soto, "Optical Biosensors and Their Applications for the Detection of Water Pollutants," *Biosensors*, vol. 13, no. 3, p. 370, Mar. 2023, doi: 10.3390/bios13030370.

[42] Q. Zhang *et al.*, "A feedback-controlling digital microfluidic fluorimetric sensor device for simple and rapid detection of mercury (II) in costal seawater," *Mar. Pollut. Bull.*, vol. 144, pp. 20–27, July 2019, doi: 10.1016/j.marpolbul.2019.04.063.

[43] J. Homola, S. S. Yee, and G. Gauglitz, "Surface plasmon resonance sensors: review," *Sens. Actuators B Chem.*, vol. 54, no. 1–2, pp. 3–15, Jan. 1999, doi: 10.1016/S0925-4005(98)00321-9.

[44] N. Díaz-Herrera, O. Esteban, M. C. Navarrete, M. L. Haitre, and A. González-Cano, "*In situ* salinity measurements in seawater with a fibre-optic probe," *Meas. Sci. Technol.*, vol. 17, no. 8, pp. 2227– 2232, Aug. 2006, doi: 10.1088/0957-0233/17/8/024.

[45] F. Colas *et al.*, "A surface plasmon resonance system for the underwater detection of domoic acid," *Limnol. Oceanogr. Methods*, vol. 14, no. 7, pp. 456–465, July 2016, doi: 10.1002/lom3.10104.

[46] T. Wriedt, "A Review of Elastic Light Scattering Theories," *Part. Part. Syst. Charact.*, vol. 15, no. 2, pp. 67–74, Apr. 1998, doi: 10.1002/(SICI)1521-4117(199804)15:2%3C67::AID-PPSC67%3E3.0.CO;2-F.

[47] F. Glöckler, F. Foschum, and A. Kienle, "Continuous Sizing and Identification of Microplastics in Water," *Sensors*, vol. 23, no. 2, p. 781, Jan. 2023, doi: 10.3390/s23020781.

[48] T. M. Squires and S. R. Quake, "Microfluidics: Fluid physics at the nanoliter scale," *Rev Mod Phys*, vol. 77, no. 3, pp. 977–1026, Oct. 2005, doi: 10.1103/RevModPhys.77.977.

[49] N.-T. Nguyen and Z. Wu, "Micromixers—a review," *J. Micromechanics Microengineering*, vol. 15, no. 2, pp. R1–R16, Feb. 2005, doi: 10.1088/0960-1317/15/2/R01.

[50] F. Wang, J. Zhu, L. Chen, Y. Zuo, X. Hu, and Y. Yang, "Autonomous and In Situ Ocean Environmental Monitoring on Optofluidic Platform," *Micromachines*, vol. 11, no. 1, p. 69, Jan. 2020, doi: 10.3390/mi11010069.

[51] L. Käse and J. K. Geuer, "Phytoplankton Responses to Marine Climate Change – An Introduction," in *YOUMARES 8 – Oceans Across Boundaries: Learning from each other*, S. Jungblut, V. Liebich, and M. Bode, Eds., Cham: Springer International Publishing, 2018, pp. 55–71. doi: 10.1007/978-3-319-932842_5.

[52] H. Liang, J. Wang, L. Zhang, J. Liu, and S. Wang, "Review of Optical Fiber Sensors for Temperature, Salinity, and Pressure Sensing and Measurement in Seawater," *Sensors*, vol. 22, no. 14, p. 5363, July 2022, doi: 10.3390/s22145363.

[53] R. Romeo, P. A. Giuliano Albo, and S. Lago, "Density and derived properties of standard seawater up to high pressure in stable and metastable states," *Deep Sea Res. Part Oceanogr. Res. Pap.*, vol. 177, p. 103624, Nov. 2021, doi: 10.1016/j.dsr.2021.103624.

[54] J. Ran *et al.*, "Quantifying the contribution of temperature, salinity, and climate change to sea level rise in the Pacific Ocean: 2005-2019," *Front. Mar. Sci.*, vol. 10, p. 1200883, Aug. 2023, doi: 10.3389/fmars.2023.1200883.

[55] G. T. McNeil, "Metrical Fundamentals of Underwater Lens System," *Opt. Eng.*, vol. 16, no. 2, Apr. 1977, doi: 10.1117/12.7972089.

[56] M. Yücel, A. D. Beaton, M. Dengler, M. C. Mowlem, F. Sohl, and S. Sommer, "Nitrate and Nitrite Variability at the Seafloor of an Oxygen Minimum Zone Revealed by a Novel Microfluidic In-Situ Chemical Sensor," *PLOS ONE*, vol. 10, no. 7, p. e0132785, July 2015, doi: 10.1371/journal.pone.0132785.

[57] M. M. Grand *et al.*, "A Lab-On-Chip Phosphate Analyzer for Long-term In Situ Monitoring at Fixed Observatories: Optimization and Performance Evaluation in Estuarine and Oligotrophic Coastal Waters," *Front. Mar. Sci.*, vol. 4, p. 255, Aug. 2017, doi: 10.3389/fmars.2017.00255.

[58] X. Cao, S. W. Zhang, D. Z. Chu, N. Wu, H. K. Ma, and Y. Liu, "A design of spectrophotometric microfluidic chip sensor for analyzing silicate in seawater," *IOP Conf. Ser. Earth Environ. Sci.*, vol. 82, p. 012080, Aug. 2017, doi: 10.1088/1755-1315/82/1/012080.

[59] S. K. Abi Kaed Bey and M. C. Mowlem, "Measurement of nano molar ammonium with a cyclic olefin copolymer microchip and low-power LED," *Sens. Bio-Sens. Res.*, vol. 43, p. 100611, Feb. 2024, doi: 10.1016/j.sbsr.2023.100611.

[60] F. M. M. Morel, A. J. Milligan, and M. A. Saito, "Marine Bioinorganic Chemistry: The Role of Trace Metals in the Oceanic Cycles of Major Nutrients," in *Treatise on Geochemistry*, Elsevier, 2003, pp. 113–143. doi: 10.1016/B0-08-043751-6/06108-9.

[61] K. W. Bruland and M. C. Lohan, "Controls of Trace Metals in Seawater," in *Treatise on Geochemistry*, Elsevier, 2003, pp. 23–47. doi: 10.1016/B0-08-043751-6/06105-3.

[62] L. Li, W. Xiaojing, L. Jihua, and S. Xuefa, "Dissolved trace metal (Cu, Cd, Co, Ni, and Ag) distribution and Cu speciation in the southern Yellow Sea and Bohai Sea, China: DISSOLVED TRACE METALS IN CHINA," *J. Geophys. Res. Oceans*, vol. 122, no. 2, pp. 1190–1205, Feb. 2017, doi: 10.1002/2016JC012500.

[63] S. C. Doney, D. S. Busch, S. R. Cooley, and K. J. Kroeker, "The Impacts of Ocean Acidification on Marine Ecosystems and Reliant Human Communities," *Annu. Rev. Environ. Resour.*, vol. 45, no. 1, pp. 83–112, Oct. 2020, doi: 10.1146/annurev-environ-012320-083019.

[64] H. Kim, A. C. Franco, and U. R. Sumaila, "A Selected Review of Impacts of Ocean Deoxygenation on Fish and Fisheries," *Fishes*, vol. 8, no. 6, p. 316, June 2023, doi: 10.3390/fishes8060316.

[65] C.-Z. Lai, M. D. DeGrandpre, and R. C. Darlington, "Autonomous Optofluidic Chemical Analyzers for Marine Applications: Insights from the Submersible Autonomous Moored Instruments (SAMI) for pH and pCO2," *Front. Mar. Sci.*, vol. 4, p. 438, Jan. 2018, doi: 10.3389/fmars.2017.00438.

[66] B. L. Preston, "Indirect Effects in Aquatic Ecotoxicology: Implications for Ecological Risk Assessment," *Environ. Manage.*, vol. 29, no. 3, pp. 311–323, Mar. 2002, doi: 10.1007/s00267-001-0023-1.

[67] D. Vergara, J. De La Hoz-M, E. A. Ariza-Echeverri, P. Fernández-Arias, and Á. Antón-Sancho, "Evaluating Solutions to Marine Plastic Pollution," *Environments*, vol. 12, no. 3, p. 86, Mar. 2025, doi: 10.3390/environments12030086.

[68] Department of Physics and Physical Oceanography, Memorial University of Newfoundland, St. John's, NL A1B 3X7, Canada, D. Zhang, L. Men, Department of Physics and Physical Oceanography, Memorial University of Newfoundland, St. John's, NL A1B 3X7, Canada, Q. Chen, and Department of Physics and Physical Oceanography, Memorial University of Newfoundland, St. John's, NL A1B 3X7, Canada, "Ocean Observation with Opto-Microfluidic Devices," *J. Environ. Inform.*, 2016, doi: 10.3808/jei.201600351.

[69] Z. Yang, C. Li, Z. Zhang, G. Lu, Z. Cai, and W. Cao, "Development of an In Situ Analyzer Based on Sequential Injection Analysis and Liquid Waveguide Capillary Flow Cell for the Determination of Dissolved Reactive Phosphorus in Natural Waters," *Sensors*, vol. 20, no. 10, p. 2967, May 2020, doi: 10.3390/s20102967.

[70] Z. Yang *et al.*, "A high-sensitivity lab-on-a-chip analyzer for online monitoring of nitrite and nitrate in seawater based on liquid waveguide capillary cells," *Lab. Chip*, vol. 24, no. 14, pp. 3528–3535, 2024, doi: 10.1039/D4LC00248B.

[71] D. Barshilia, L.-K. Chau, and G.-E. Chang, "Low-cost planar waveguide-based optofluidic sensor for real-time refractive index sensing," *Opt. Express*, vol. 28, no. 19, p. 27337, Sept. 2020, doi: 10.1364/OE.400800.

[72] J. Homola, "Surface Plasmon Resonance Sensors for Detection of Chemical and Biological Species," *Chem. Rev.*, vol. 108, no. 2, pp. 462–493, Feb. 2008, doi: 10.1021/cr068107d.

[73] G. Pandraud, T. M. Koster, C. Gui, M. Dijkstra, A. Van Den Berg, and P. V. Lambeck, "Evanescent wave sensing: new features for detection in small volumes," *Sens. Actuators Phys.*, vol. 85, no. 1–3, pp. 158–162, Aug. 2000, doi: 10.1016/S0924-4247(00)00367-8.

[74] E. Benito-Peña, M. G. Valdés, B. Glahn-Martínez, and M. C. Moreno-Bondi, "Fluorescence based fiber optic and planar waveguide biosensors. A review," *Anal. Chim. Acta*, vol. 943, pp. 17–40, Nov. 2016, doi: 10.1016/j.aca.2016.08.049.

[75] M. Zhao, H. Tang, Z. Liu, Z. Tong, and Z. Qi, "A Surface-Scattering-Based Composite Optical Waveguide Sensor for Aerosol Deposition Detection," *Chemosensors*, vol. 10, no. 12, p. 535, Dec. 2022, doi: 10.3390/chemosensors10120535.

[76] F. Geißler *et al.*, "Evaluation of a Ferrozine Based Autonomous in Situ Lab-on-Chip Analyzer for Dissolved Iron Species in Coastal Waters," *Front. Mar. Sci.*, vol. 4, p. 322, Oct. 2017, doi: 10.3389/fmars.2017.00322.

[77] A. G. Vincent *et al.*, "Nitrate drawdown during a shelf sea spring bloom revealed using a novel microfluidic in situ chemical sensor deployed within an autonomous underwater glider," *Mar. Chem.*, vol. 205, pp. 29–36, Sept. 2018, doi: 10.1016/j.marchem.2018.07.005.

[78] A. Schaap *et al.*, "Quantification of a subsea CO2 release with lab-on-chip sensors measuring benthic gradients," *Int. J. Greenh. Gas Control*, vol. 110, p. 103427, Sept. 2021, doi: 10.1016/j.ijggc.2021.103427.